**Supporting Information**

# Highly Efficient Porous Conductive Polymer Electrode for Seawater Desalination

Wenfei Wei,[a,b] Wensong Zou,[a] Dazhong Yang,[a,b] Renji Zheng,[a,b] Ranhao Wang,[a] and Hong Chen[a,*]

a. State Environmental Protection Key Laboratory of Integrated Surface Water-Groundwater Pollution Control, Guangdong Provincial Key Laboratory of Soil and Groundwater Pollution Control, School of Environmental Science and Engineering, Southern University of Science and Technology, Shenzhen 518055, China.

b. National Engineering Laboratory for Methanol to Olefins, Dalian National Laboratory for Clean Energy, Dalian Institute of Chemical Physics, Chinese Academy of Sciences, Dalian 116023, China.

Corresponding author: chenh3@sustech.edu.cn

## 1. Electrochemical measurement for acetylene black and polyvinylidene difluoride (PVDF)

The removal capacity contributed by acetylene black and PVDF in working electrode needs to be taken into consideration. To eliminate their contribution to battery desalination, we prepared an electrode made of acetylene black and PVDF with a mass radio of 60:40. As shown in Figure S1a, this electrode shows rectangular-shaped CVs, which indicate a capacitive behavior. The specific discharge capacities of acetylene black and PVDF is 5-6 mAh $g^{-1}$ (Figure S1b). The low capacity has been used to calibrate the data when calculate the specific capacity of PAQS in the later cycling progress.

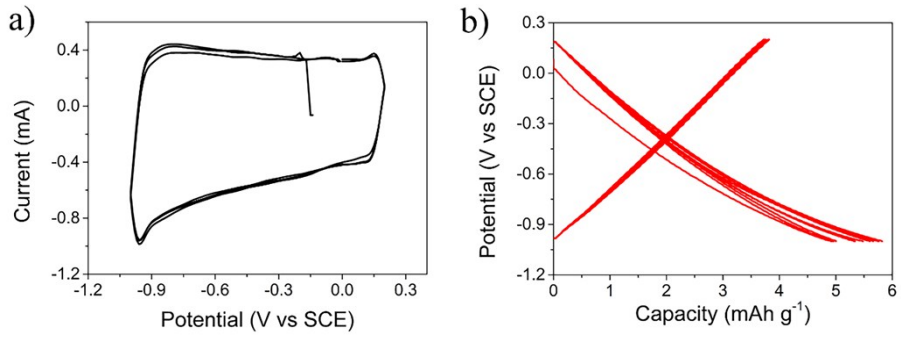


Figure S1. Electrochemical performance of acetylene black. a) CV of acetylene black at 1 mV $s^{-1}$. b) Charge and discharge curves of acetylene black /PVDF electrode in 0.5 M NaCl at 60 mA $g^{-1}$.

## 2. The ions concentration in the natural seawater

The concentration of ions contained in natural seawater is determined by ICP-OES and ion chromatography.

Table S1. Characteristics of reference standard and Shenzhen Bay area seawater used in this study.

| Chemical ion (mg $L^{-1}$) | $Na^+$ | $Mg^{2+}$ | $Ca^{2+}$ | $K^+$ | $Cl^-$ | $SO_4^{2-}$ | $Br^-$ | pH |
|---|---|---|---|---|---|---|---|---|
| Seawater [a] | 10752 | 1295 | 416 | 390 | 19345 | 2701 | 66 | |
| Shenzhen Bay seawater | 13472 | 2826 | 842 | 659 | 18713 | 2754 | 46 | 7.95 |

[a] Range of values taken from Lesley Joseph et al.[1]

## 3. Characterization of the electrodes

The conductivity of the electrode materials can be confirmed using electrochemical impedance spectroscopy (EIS). Based on the EIS data, the charge transfer resistance ($R_{ct}$) is consistent with the electrochemical reaction resistance. Low charge transfer resistance reveals the facile electron transfer within material. The pure PAQS powder has been pressed into a tablet electrode for EIS measurement. As shown in Figure S2a, the $R_{ct}$ of PAQS is 10.1 Ω, which indicates that PAQS could exhibits a fast cations and e- diffusion during the electrochemical reaction process. The $R_{ct}$ of working electrode (PAQS + acetylene black + PVDF) (initial: 8.9 Ω) used in BDI experiment is lower than pure PAQS electrode due to contribution of conductive acetylene black (Figure S2b). These values are lower than the reported $R_{ct}$ of other materials (Table S2).[2-15]

SEM and $N_2$ adsorption-desorption are used to characterize a piece of prepared electrode. As shown in Figure S2c, the acetylene black (~50 nm) is uniformly adhered to the PAQS surface, and there are also a lot of porosity within the electrode. The $N_2$ adsorption-desorption isotherm of electrode can be described to be the type-Ⅳ isotherm with H3 hysteresis loops (at p/po > 0.4) with a hierarchal porous structure feature. The specific Brunauer-Emmett-Teller (BET) surface area is 81.8 $m^2 g^{-1}$, and the pore sizes mainly distribute range from 3 to 20 nm. The specific BET surface area of electrode (81.8 $m^2 g^{-1}$) is higher that PAQS (59.8 $m^2 g^{-1}$). Which might be contributed by the ~50 nm acetylene black. According the results of SEM and $N_2$ adsorption-desorption isotherm of electrode, we can interpret that PVDF may have a mild impact on the structure and performance of the final working electrode.

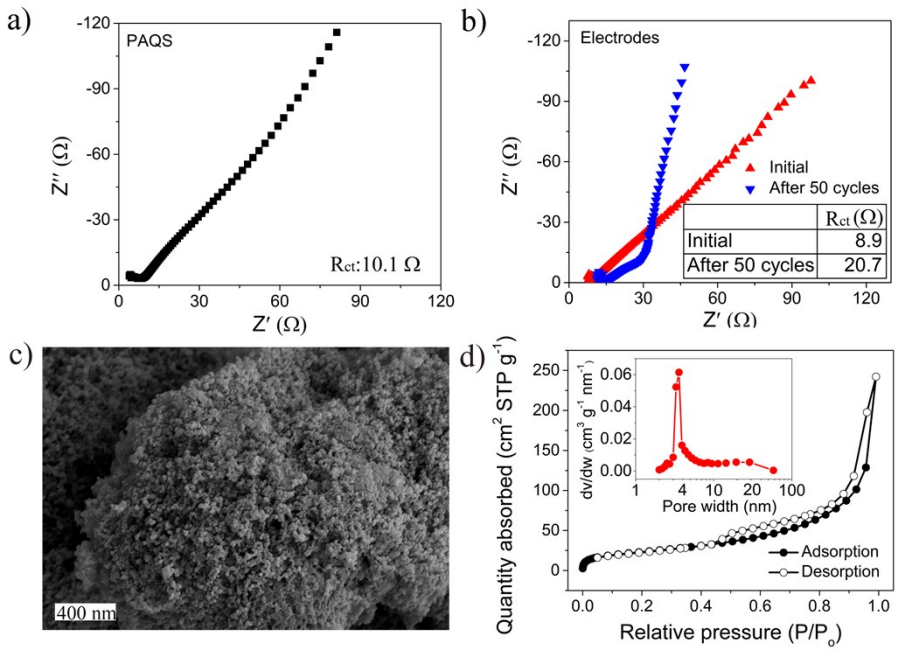


Figure S2. a) Nyquist plots of pure PAQS. b) Nyquist plots of PAQS involved working electrode. c) SEM image and d) $N_2$ adsorption-desorption curve of PAQS involved working electrode.

Table S2. $R_{ct}$ of some typical electrode materials.[2-15]

| Material | Vat Green 8 [2] | Poly (2-chloro-3,5,6-trisulfide-1,4-benzoquinone [3] | Silver terephthalate [4] | poly (2,2,6,6-tetramethyl-1piperidinyloxy -4-yl methacrylate) [5] | Polyimide [6] |
|---|---|---|---|---|---|
| $R_{ct}$ (Ω) | 37 | 60 | 79 | 100 | 133 |
| Material | poly(1,4-anthraquinone) [7] | poly(2,5-dihydroxy-p-benzoquinonyl sulfide) [8] | poly{[N,N′-bis(2-octyldodecyl)-1,4,5,8-naphthalenedicarboximide-2,6-diyl]-alt-5,5′-(2,2′-bithiophene)} [9] | pyromellitic dianhydride-tris(2-aminoethyl)amine [10] | poly(2,5-dihydroxyl-1,4-benzoquinonyl sulfide) [11] |
| $R_{ct}$ (Ω) | 188 | 200 | 206 | 415 | 1458 |
| Material | $LiFePO_4$ [12] | $LiCoO_2$ [13] | $Na_{0.44}MnO_2$ [14] | $NaTi_2(PO_4)_3$ [15] | |
| $R_{ct}$ (Ω) | 522 | ~ 750 | ~ 250 | ~ 260 | |

## 4. Charge storage mechanism of PAQS electrode

Here, we used the scan-rate-dependent CV curves to quantify the contribution from capacitive effects (both surface pseudocapacitance and double-layer capacitance) and diffusion-controlled cations insertion process to the current response according to the following equation: [16–18]

$$i\,(V) = k_1 v + k_2 v^{1/2}$$

Where $v$ is the sweep rate, $i(V)$ is the current response at a fixed potential $(V)$, $k_1 v$ is the current due to capacitive effects, $k_2 v$ is the current due to diffusion-controlled insertion process. By determining both $k_1$ and $k_2$, it is thus possible to distinguish the fraction of the current arising from cations insertion and that from capacitive processes at specific potential. The capacitive and diffusion-controlled contributions to charge storage are shown in Figure S3a and 3b. For PAQS electrode, the capacitive contribution is 7.4 % and diffusion-controlled contribution is 92.6 % at 20 mV $s^{-1}$. As shown in Figure S3, the diffusion-controlled contribution is 95.6 %, 95.8 %, 94.6 %, and 93.9 % at 1 mV $s^{-1}$, 2 mV $s^{-1}$, 5 mV $s^{-1}$, and 10 mV $s^{-1}$. These values are much higher than the values of capacitive contribution. Hence, we may conclude that Faradaic ions storage (diffusion-controlled cations insertion process) play the major role in PAQS electrode for removing cations.

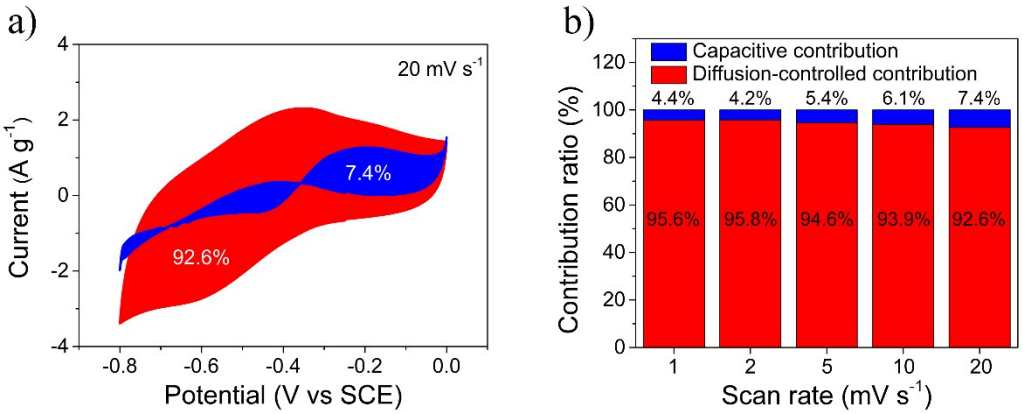


Figure S3. Quantitative capacitive analysis of sodium storage behavior. a) Capacitive contribution (7.4 %) and diffusion contribution (92.6 %) at 20 mV $s^{-1}$, b) Normalized contribution ratio of capacitive capacities at different scan rates.

## 5. PAQS electrode evolution after discharging

To grasp further insights into electrochemical reaction mechanism, we have monitored the material evolution by ex -situ FT-IR. As shown in Figure S4, the C=O band at 1676 $cm^{-1}$ is disappeared. Moreover, the new band at around 1363 $cm^{-1}$ belongs to the stretching vibration of the -C-$O^-$ $M^{n+}$ ($Na^+$, $K^+$, $Mg^{2+}$ and $Ca^{2+}$) is presented in the discharged form of PAQS.[19] The changes observed in the spectra confirmed that carbonyl group is the active sites, which could binding with metal ions.

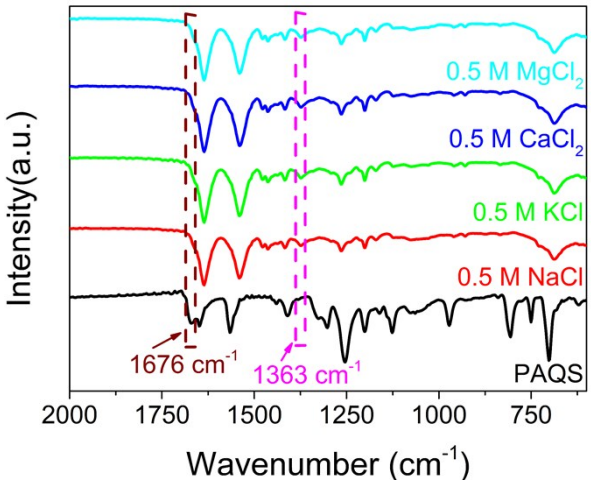


Figure S4. FT-IR spectra of the discharged electrodes.

## 6. Structure characterization of PAQS electrodes and phase analysis

As shown in Figure S5a, the diffraction peaks appear at 12° and 24° further confirms the successful synthesis of PAQS.[20] The discharged electrode at -1 V and the charged electrode at 0 V shows a similar XRD pattern as the fresh electrode. It indicates that PAQS preserves its amorphous structure during ions insertion and extraction process. The XRD pattern of discharged electrodes at different electrolytes are shown in Figure S5b. All of them preserves the broad diffraction peak at 24° which has been contributed by PAQS. The difference between the discharged electrodes in 0.5 M $MCl_2$ ($MgCl_2$, $CaCl_2$) and 0.5 M MCl (NaCl, KCl) are the existence of new diffraction peaks. $Mg(OH)_2$ phase appeared after discharged in 0.5 M $MgCl_2$ solution. In 0.5 M $CaCl_2$ solution, the discharged electrodes $Ca(OH)_2$ and $CaCO_3$ are present. The formation of precipitate during the discharge-charge reaction process is attributed to the increasing of pH value. The pH value of the electrolyte solution has been increased slightly to around 7.0-8.0 due to the following depolarization reaction and parasitic reactions during the charging progress.[21]

$$\frac{1}{2} O_2 + e^- + H^+ \rightarrow \frac{1}{2} H_2O_2 \qquad E_0 = 0.69 \text{ V / SHE} \tag{1}$$

$$\frac{1}{2} H_2O_2 + e^- + H^+ \rightarrow H_2O \qquad E_0 = 1.78 \text{ V / SHE} \tag{2}$$

$$\text{PAQS-} M^{2+} + \frac{1}{2} O_2 + H_2O \rightarrow \text{PAQS} + M^{2+} + 2\ OH^- \tag{3}$$

When the pH of the solution increased, the following reactions happened in 0.5 M $MgCl_2$ and 0.5 M $CaCl_2$.

$$Mg^{2+} + OH^- \rightarrow Mg(OH)_2 \tag{4}$$

$$Ca^{2+} + OH^- \rightarrow Ca(OH)_2 \tag{5}$$

$$Ca^{2+} + CO_2 + 2OH^- \rightarrow CaCO_3 + H_2O \tag{6}$$

Therefore, different crystalline phases have been precipitated in different electrolytes. Such as $Mg(OH)_2$ in 0.5 M $MgCl_2$; $Ca(OH)_2$ and $CaCO_3$ in 0.5 M $CaCl_2$. Herein, the electrolytes of 0.5 M $MgCl_2$ and 0.5 M $CaCl_2$ are used in the electrochemical study. Although the beneficial chemical reactions to form $Mg(OH)_2$ and $Ca(OH)_2$ and $CaCO_3$ can remove $Mg^{2+}$ and $Ca^{2+}$ in water solution, they are fundamentally different from electrochemical reactions. We need to further confirm that if PAQS used in seawater desalination by electrochemical reaction to remove $Mg^{2+}$

and $Ca^{2+}$. As we know, the solubility product of a substance is affected by ions concentration. We further confirmed the XRD of discharged electrode in low concentration electrolytes, with monocation solution of a concentration of 0.05 M and 0.01 M (the concentration of single cations is closed to the observed data in Table S1), mixed chloride salts solution and Shenzhen Bay seawater. As shown in Figure S5c, the electrodes have a pair of board redox peaks in low concentration NaCl electrolytes, that confirms that PAQS have the redox activity in low concentration electrolytes. The XRD patterns of the discharged electrodes have been collected as shown in Figure S5d, only the discharged electrode (0.05 M $MgCl_2$) shows a diffraction peak at 38° which might be corresponding to the phase of $Mg(OH)_2$. When using the mixed chloride solution and Shenzhen Bay seawater as the electrolytes, the discharged electrode without any chemical reaction precipitation. This result indicates that low concentration salt cations inserted into the PAQS electrode mainly through binding with carbonyl group rather than the other condensation or precipitate reaction.

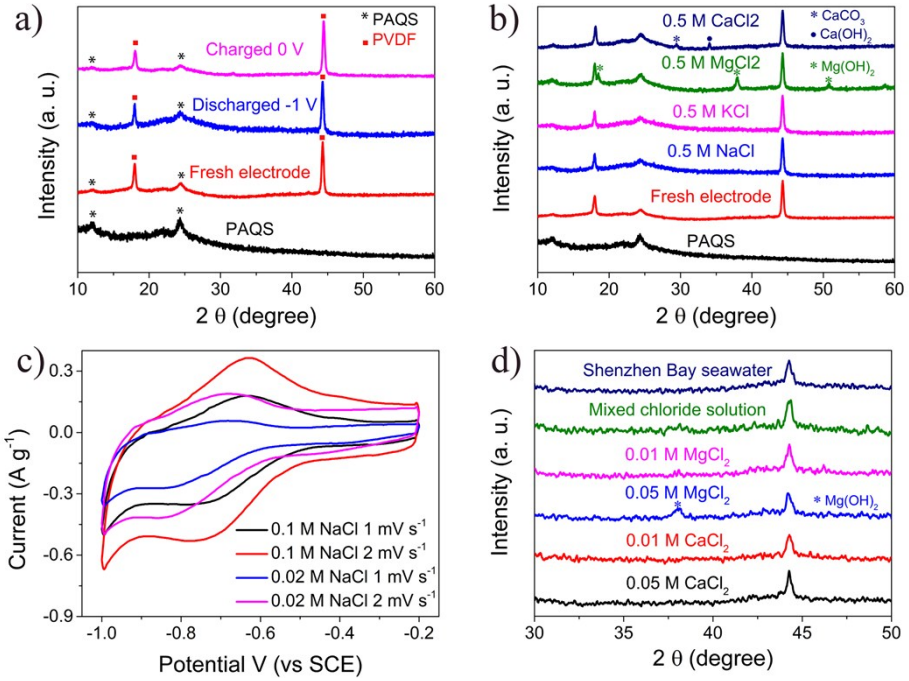


Figure S5. Phase analysis of PAQS electrodes. a) XRD of electrodes in different state (the electrolyte is 0.5 M NaCl). b) XRD of discharged PAQS electrodes in different 0.5 M electrolytes. c) CV curves of PAQS in 0.1 M NaCl and 0.02 M NaCl. d) XRD of electrodes in different electrolytes.

## 7. Discharge curves of PAQS electrodes in different electrolytes

The specific capacity was obtained during the charging and discharging of the electrode in the battery cycling system. It includes charge specific capacity part and discharge specific capacity part. When calculating the ions removal capacity of the PAQS electrode, we used the discharge specific capacity (discharging curve), which corresponds to cations insertion process.

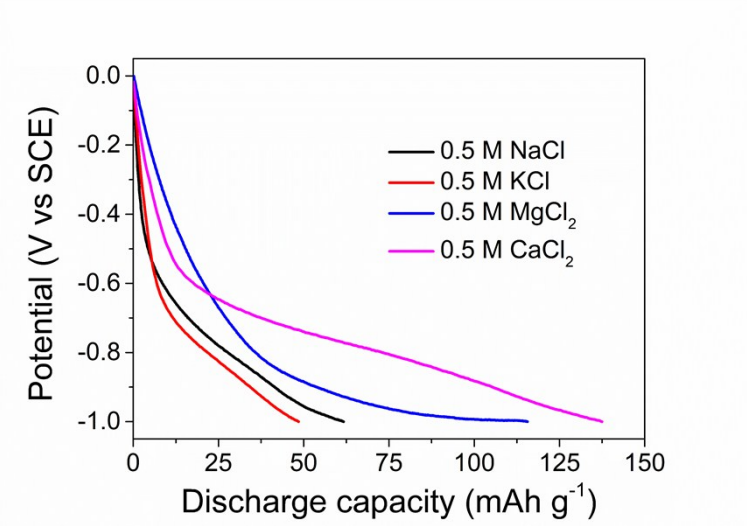


Figure S6. Discharge curves of PAQS electrodes in 0.5 NaCl, 0.5 M KCl, 0.5 M $MgCl_2$, 0.5 M $CaCl_2$.

## 8. Elemental mapping of PAQS electrode

The EDS mapping of PAQS discharged in mixed chloride salt solution further confirms that PAQS can remove multiple metal cations. As shown in Figure S7, the contents of Na and Mg elements in the discharged PAQS electrode is much higher than K and Ca. The element difference distribution in EDS mapping of $Na^{+}$, $Mg^{2+}$ with $K^{+}$, $Ca^{2+}$ may be due to the higher removal capacity of $Na^{+}$, $Mg^{2+}$ in mixed chloride salts solution.

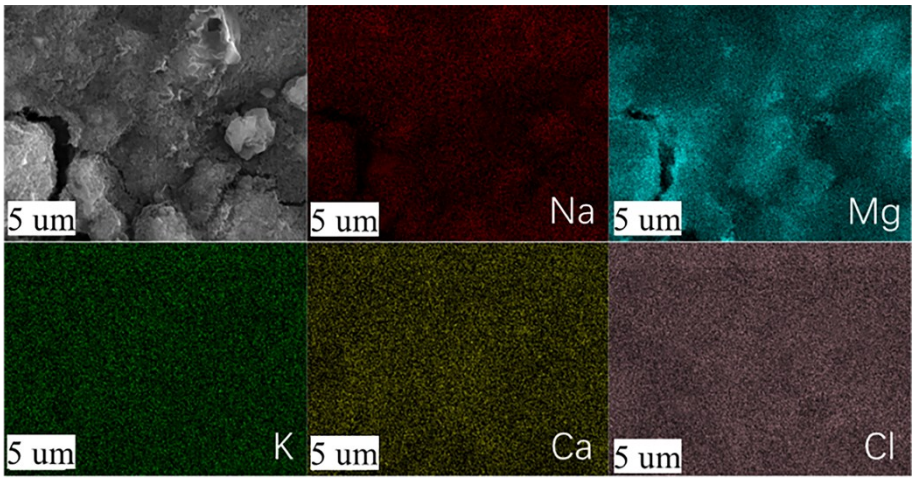


Figure S7. EDS mapping of the PAQS electrode after discharge to -1.0 V in artificial mixed chloride salts solution.

## 9. Optimal conditions for electrochemical reaction used in desalination system

To find out the best working potential conditions of the asymmetric cell, we studied the electrochemical performance of PAQS electrode in 0.5 M NaCl solution. For all test, the mass of active carbon is excessive for fully studying PAQS deionization performance. First, we study the specific capacity and coulombic efficiency for full battery in different voltage. As shown in Figure S8a, in the full battery system, the coulombic efficiency (CE) is 123 % in -1.2 - 1.2 V. When the voltage is -1.0 - 1.0 V, CE reached 99.5 %, the capacity is 38 mAh $g^{-1}$. Here, the value of coulombic efficiency is closed to 100 %, it means the electrochemical reaction is reversible and minor side-reaction happens. As we can see in Figure S8a, the battery system has a suitable coulombic efficiency and a high specific capacity in -1.0 - 1.0 V. To further evaluate PAQS deionization performance at different current, we study the full battery system rate performance in -1.0 - 1.0 V (Figure S8b). PAQS exhibited a specific capacity of 40 mAh $g^{-1}$ at a current rate of 60 mA $g^{-1}$. When the current rate was increased 20-fold (1200 mA $g^{-1}$), a specific capacity of 28 mAh $g^{-1}$ was observed, indicating the ideal rate capability of PAQS. Moreover, the coulombic efficiency is 99.6 % at 1200 mA $g^{-1}$. So, the full battery system seawater deionization performance has been selected within a voltage window of -1 to 1 V.

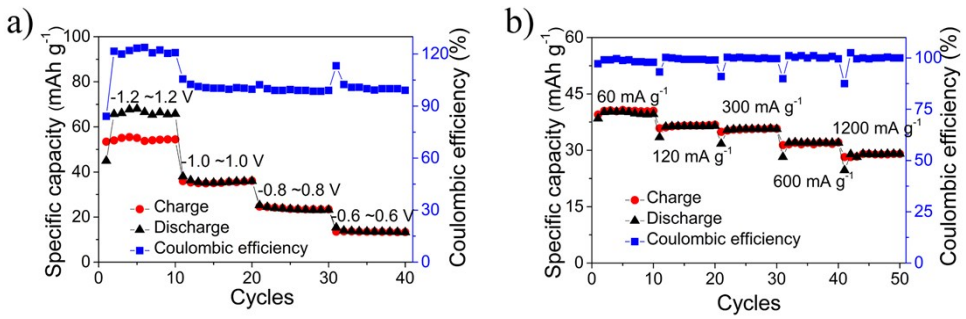


Figure S8. Optimal conditions for electrochemical reaction in desalination system. a) PAQS cycle performance in different voltage at 60 mA $g^{-1}$ (0.5 M NaCl). b) PAQS rate performance at -1~1 V (0.5 M NaCl).

## 10. Anion removal capacity

The anions removal capacity of counter electrode was shown in Figure S9. The $Cl^-$ by counter electrode in mixed chloride solution is 10.3 mg $g^{-1}$. The removal capacity of $Cl^-$, $SO_4^{2-}$ and $Br^-$ is 9.9 mg $g^{-1}$, 0.9 mg $g^{-1}$ and 0.1 mg $g^{-1}$, respectively.

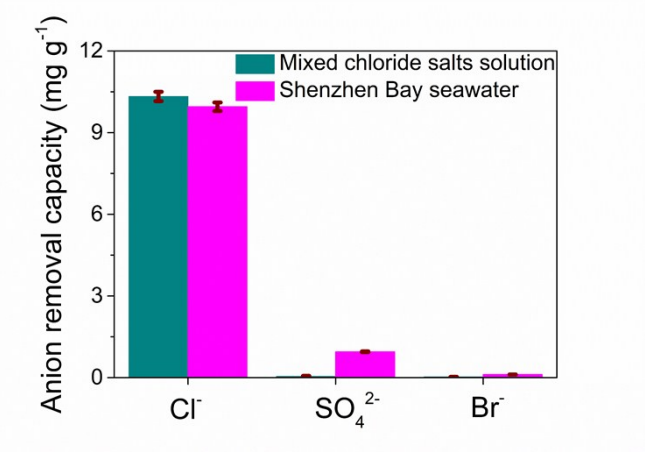


Figure S9. Anions removal capacity of the counter electrode in mixed chloride salts solution and Shenzhen Bay seawater.

Note: The different metal ions remove capacity of PAQS in mixed chloride salts solution and Shenzhen Bay seawater has been discussed here.

As discussed in Figure 3a, $Na^+$ will be first insert into PAQS when the electrolytes have the same metal ions concentration in discharging process. As the potential decreasing, $K^+$, $Mg^{2+}$ and $Ca^{2+}$ will be inserted accordingly. According to the Nernst function, there is a positive correlation between reduction potential of PAQS and cations concentration, the insert potential of $K^+$, $Mg^{2+}$and $Ca^{2+}$ will reduce in seawater compare with 0.5 M single metal ions solution. As shown in Figure S3c, the reduction potential of PAQS has reduced compared with 0.5 M NaCl (-0.85 V in 0.02 M NaCl, -0.73 V in 0.1 M NaCl, -0.58 V in 0.5 M NaCl). Due to the higher concentration of $Mg^{2+}$ and $Ca^{2+}$ than $K^+$ in seawater, the insert potential of $Mg^{2+}$ and $Ca^{2+}$ may be higher than $K^+$. In mixed chloride solution and Shenzhen Bay seawater, $Na^+ > Mg^{2+} > Ca^{2+} > K^+$, may be the sequential relationship of the reduction potential. So, the metal ions remove capacity of PAQS working electrode for $Na^+$, $Mg^{2+}$, $Ca^{2+}$ and $K^+$ are different when we mainly explore the cations removal capacity (mg $g^{-1}$) of PAQS in discharge process at a current rate of 60 mA $g^{-1}$.

Table S3. TOC analysis of electrolytes in different state

| | 0.5 M NaCl [a] | 0.5 M NaCl [b] | 0.5 M NaCl [c] | Shenzhen Bay seawater [a] | Shenzhen Bay seawater [b] | Shenzhen Bay seawater [c] |
|---|---|---|---|---|---|---|
| C mg $L^{-1}$ | 11.45 | 11.45 | 11.79 | 8.91 | 9.51 | 9.74 |
| m mg | 0.05725 | 0.05725 | 0.05895 | 0.04455 | 0.04755 | 0.04870 |

[a] The electrolyte directly exposed to air for 72 h.

[b] PAQS electrode immersed in the electrolyte and then exposed to air for 72 h.

[c] The electrolyte was collected after 50 cycles.

**References**


1 L. Joseph, J. Heo, Y. G. Park, J. R. V. Flora and Y. Yoon, *Desalination*, 2011, **281**, 68–74.

2 W. Ai, W. Zhou, Z. Du, C. Sun, J. Yang, Y. Chen, Z. Sun, S. Feng, J. Zhao, X. Dong, W. Huang and T. Yu, *Adv. Funct. Mater.*, 2017, **27**, 1–9.

3 W. Wei, L. Li, L. Zhang, J. Hong and G. He, *Mater. Lett.*, 2018, **213**, 126–130.

4 J. Xue, C. Fan, Q. Deng, M. Zhao, L. Wang, A. Zhou and J. Li, *Electrochim. Acta*, 2016, **219**, 418–424.

5 Y. Kim, C. Jo, J. Lee, C. W. Lee and S. Yoon, *J. Mater. Chem.*, 2012, **22**, 1453–1458.

6 A. Ahmad, H. Wu, Y. Guo, Q. Meng, Y. Meng, K. Lu, L. Liu and Z. Wei, *RSC Adv.*, 2016, **6**, 33287–33294.

7 Z. Song, Y. Qian, M. L. Gordin, D. Tang, T. Xu, M. Otani, H. Zhan, H. Zhou and D. Wang, *Angew. Chemie - Int. Ed.*, 2015, **54**, 13947–13951.

8 Z. Song, Y. Qian, X. Liu, T. Zhang, Y. Zhu, H. Yu, M. Otani and H. Zhou, *Energy Environ. Sci.*, 2014, **7**, 4077–4086.

9 Y. Liang, Z. Chen, Y. Jing, Y. Rong, A. Facchetti and Y. Yao, *J. Am. Chem. Soc.*, 2015, **137**, 4956–4959.

10 H. Wu, Q. Meng, Q. Yang, M. Zhang, K. Lu and Z. Wei, *Adv. Mater.*, 2015, **27**, 6504–6510.

11 K. Amin, Q. Meng, A. Ahmad, M. Cheng, M. Zhang, L. Mao, K. Lu and Z. Wei, *Adv. Mater.*, 2018, **30**, 1–8.

12 Y. Li, J. Wang, H. X. Huang, J. Wang, M. Zhang and Mm. M. Liang, *Adv. Powder Technol.*, 2019, **30**, 1442–1449.

13 J. Zhao, L. Wang, X. He, C. Wan and C. Jiang, *Int. J. Electrochem. Sci.*, 2010, **5**, 478–488.

14 D. J. Kim, R. Ponraj, A. G. Kannan, H. W. Lee, R. Fathi, R. Ruffo, C. M. Mari and D. K. Kim, *J. Power Sources*, 2013, **244**, 758–763.

15 M. Li, L. Liu, P. Wang, J. Li, Q. Leng and G. Cao, *Electrochim. Acta*, 2017, **252**, 523–531.

16 D. Chao, P. Liang, Z. Chen, L. Bai, H. Shen, X. Liu, X. Xia, Y. Zhao, S. V. Savilov, J. Lin and Z. X. Shen, *ACS Nano*, 2016, **10**, 10211–10219.

17 T. Brezesinski, J. Wang, S. H. Tolbert and B. Dunn, *Nat. Mater.*, 2010, **9**, 146–151.

18 X. Xia, D. Chao, Y. Zhang, J. Zhan, Y. Zhong, X. Wang, Y. Wang, Z. X. Shen, T. Jiangping and H. J. Fan, *Small*, 2016, **12**, 3048–3058.

19 A. Vizintin, J. Bitenc, A. Kopač Lautar, K. Pirnat, J. Grdadolnik, J. Stare, A. Randon-Vitanova and R. Dominko, *Nat. Commun.*, 2018, 7, 1-7.

20 Z. Jian, Y. Liang, I. A. R. Pérez, Y. Yao and X. Ji, *Electrochem. Commun.*, 2016, **71**, 5–8.

21 Y. Li, Z. Ding, J. Li, J. Li, T. Lu and L. Pan, *Desalination*, 2019, **469**, 114098.